Journal of Wind Engineering & Industrial Aerodynamics 167 (2017) 1–12

Contents lists available at ScienceDirect

Journal of Wind Engineering & Industrial Aerodynamics

journal homepage: www.elsevier.com/locate/jweia

Aerodynamic design methodology for wind tunnel tests of wind turbine rotors

Ilmas Bayati, Marco Belloli*, Luca Bernini, Alberto Zasso

Politecnico di Milano, Department of Mechanical Engineering, Italy

ARTICLE INFO

Keywords:
Wind turbines
Aero-elastic scaling
Carbon-fibre
Wind tunnel

ABSTRACT

This paper illustrates the methodology and the experimental verification of the design of a 1/75 aero-elastic scaled rotor of the DTU 10 MW reference wind turbine for wind tunnel tests. The aerodynamic design was focused on the minimization of the difference, in terms of thrust coefficient, with respect to the full scale reference. From the Selig low-Reynolds airfoils database, the SD7032 one was chosen for this purpose and a corresponding constant section wing was tested at DTU red wind tunnel, providing force and distributed pressure coefficients for the design, in the Reynolds range $30- 250 \times 10^3$ and for different angles of attack. The aero-elastic design algorithm was set to define the optimal spanwise thickness over chord ratio (t/c), the chord length and the twist, in order to match at least the first flapwise scaled natural frequency. An aluminium mould for the carbon fibre autoclave process was CNC manufactured based on B-Splines CAD definition of the external geometry given as an output of the design procedure. Wind tunnel tests at were carried out Politecnico di Milano on the whole 1/75 wind turbine scale model, confirming the successful aerodynamic design and manufacturing approaches. The experimental modal analysis carried out to verify the structural consistency of the scaled blade is also reported.

1. Introduction

Wind tunnel tests of wind turbine scale models represent an affordable and effective way for assessing the aerodynamics of wind turbines saving time, costs and uncertainties related to full scale experimentation. However, the main limitation in rotor scaling procedure for wind tunnel tests is the impossibility of matching Reynolds number with respect to full scale. This paper illustrates the non-trivial aero-elastic optimal design, the realization and the experimental verification of the wind tunnel 1/75 scale rotor of the DTU 10 MW wind turbine. More specifically, this work was developed for floating offshore wind turbine (FOWT) applications (Lifes50+, Bayati et al., 2013, 2014); nevertheless, the methodology reported and the conclusions drawn are of general validity in scaling rotors of wind turbines.

Similar efforts in scaling wind turbines have been recently made (Bredmose, 2014). Furthermore, a deep analysis of the scaling effects can be found in (Bottasso et al., 2014) regarding previous activities at Politecnico di Milano wind tunnel: this work deals with the definition of a procedure for aero-elastic model design, and good results, in term of thrust and torque value matching, were obtained as well as a correctly scaled blade structural behaviour also considering bend-twist scaling (Campagnolo et al., 2014).

A further study on the scaling effect of the turbine rotor aerodynamics was carried out in (Make, 2014), where it was found, both numerically and experimentally, that the Reynolds discrepancy caused a different behaviour of the model scale rotor, and by adjusting the chord length by an increment of 25% was obtained so that the model rotor matched target scaled thrust.

Similar results were obtained by DTU in (Bredmose et al., 2015), also in this case the rotor blades were geometrically adjusted in order to overcome the Reynolds scaling limit which, together with the use of low Reynolds airfoil and turbulence generators, allowed to obtain good results for the rotor aerodynamic performance.

The Reynolds scaling problem is even more important when dealing with offshore related testing, in this case Froude scaling is mandatory (Bredmose, 2014) worsening the Reynolds mismatch.

The DTU 10 MW wind turbine, which is the reference of this work, was firstly designed in the framework of the Light Rotor project in 2012 (Bak et al., 2012), starting from the upscaling of the reference 5 MW turbine from NREL (Jonkman et al., 2009). Later the Light Rotor project design evolved in the nowadays publicly available reference design, released by DTU (Baket al, 2013). The DTU 10 MW is being used as reference design in numerous current research activities related to wind energy development, ranging from wind farm optimization to offshore

* Corresponding author.

http://dx.doi.org/10.1016/j.jweia.2017.05.004
Received 15 February 2017; Received in revised form 9 May 2017; Accepted 10 May 2017
Available online xxxx

Table 1
DTU 10 MW turbine specifications.

Parameter	value	units
Cut in wind speed	4	m/s
Cut out wind speed	25	m/s
Rated wind speed	11.4	m/s
Rotor Diameter	178.3	m
Hub Diameter	5.6	m
Hub Height	119.0	m
Minimum Rotor Speed	6.0	rpm
Maximum Rotor Speed	9.6	rpm
Blade Prebend	3.332	m
Rotor Mass	228,0	tonn
Nacelle Mass	446,0	tonn
Tower Mass	628,4	tonn

Table 2
Wind Tunnel Model turbine specifications.

Parameter	value	units	scale
Cut in wind speed	2	m/s	$\lambda_V = 2$
Cut out wind speed	12.5	m/s	$\lambda_V = 2$
Rated wind speed	5.7	m/s	$\lambda_V = 2$
Rotor Diameter	2.37	m	$\lambda_L = 75$
Maximum Rotor Speed	360	rpm	$\lambda_f = \lambda_L \lambda_V^{-1} = 37.5$
Rotor Mass	0.54	kg	$\lambda_M = \lambda_L^3 = 4.22 \times 10^5$

wind turbine simulation or also for numerical tools benchmark and validation. Table 1 reports the main DTU 10 MW specifications in term of dimensions, masses and operating wind speed.

2. Scaling the reference design

The first step of model design was the comparison between the turbine specifications and the Polimi Wind Tunnel (GVPM) (Zasso et al., 2005) test section dimensions and flow performance. The GVPM is a closed circuit facility with two test rooms: a 4 × 4m high speed low turbulence and a 14 × 4m low speed boundary layer test section. The high speed section is characterized by very low turbulence, $Iu < 0.15\%$, and high speed, maximum velocity of 55 m/s, in the low speed section the turbulence index is higher, $Iu < 2\%$, with a reduced maximum velocity 15 m/s. The low speed section is 36 m long, 14 m wide and 4 m high, allowing very large scale wind engineering tests, useful for civil engineering application or low blockage aerodynamic related tests. Trying to avoid an excessive miniaturization of the turbine model components, the wind tunnel tests are performed in the low speed section.

In Eq. (1) the scale factor is defined as the ratio between a general DTU 10 MW turbine parameter and the corresponding wind tunnel model parameter.

$$\lambda = \frac{p_{reference}}{p_{model}} \tag{1}$$

The dimensional analysis technique is fundamental in model design for wind tunnel. A series of non-dimensional groups are usually taken into account, the most used are the Reynolds number, Froude Number, Strouhal Number, Cauchy number, etc. Usually the length scale, λ_L, is defined from simple considerations about the wind tunnel dimension, then one of the non-dimensional group is selected to be kept constant from full scale to model scale. The choice is made considering which are the most important parameters that influence tests results. For example Froude scaling is typically used for the presence of non-negligible gravity dependant loads (e.g. long-span bridges, hydrodynamic forces). In floating offshore wind turbine scale tests in ocean basins, Froude scaling is mandatory due to the presence of physical waves. Froude number is defined as in Eq. (2)

$$Fr = \frac{V}{\sqrt{gL}} \tag{2}$$

where V is the velocity, g is the gravitational acceleration and L is the length. Fixing the length scale factor λ_L due to the dimension of the model, the velocity scale factor λ_V is consequently defined as $\sqrt{\lambda_L}$, resulting in very low speeds for the tests.

For this particular project the λ_L has to be selected in the range: 70−90, the lower limit comes from the maximum wind tunnel model diameter of 2.5 m, this ensures that the blade tip is far enough from the tunnel ceiling and floor during the rotor revolution, thus avoiding the wall boundary layer. The higher limit avoids to have an excessive miniaturization of the model components.

The λ_V has a fixed range of possible values: 1.5− 3, due to a comparison between the cut out speed, 25 m/s, of the DTU 10 MW and the maximum wind tunnel speed, 15 m/s.

A discrete number of possible combinations for the scales were evaluated, a good compromise was found in $\lambda_L = 75$ and $\lambda_V = 2$. Once defined the length and velocity scales, the scales of the principal physical quantities were derived from dimensional analysis. Table 2 reports the most important scaled turbine characteristics.

The blade design aims at matching as close as possible the scaled values of the turbine aerodynamic thrust and torque. It is worth mentioning that, since this scaled design is related to the study of a floating system, the thrust matching is of higher importance since the floating system dynamics is more influenced by thrust than torque (Bredmose et al., 2015).

3. Wind tunnel model blade design input

In this scenario, the main goals in the blade design can be summarized as follows:

- matching the reference thrust coefficient
- matching the scaled first blade flapwise natural frequency
- matching the scaled blade weight

It is pretty clear that the blade design is challenging both from an aerodynamic and structural point of view. In Fig. 1 the blade design procedure is reported.

3.1. Reference design input

The DTU 10 MW reference and wind tunnel model turbine operational parameters are reported in Table 3, as combinations of wind speed, V, rotor rotational speed, Ω and Tip Speed Ratio, TSR ($TSR = \Omega \cdot R/V$). The model wind speed operational value are reduced by λ_V and the model rotational speed is reduced by λ_V/λ_L, this ensures that the TSR does not change when scaling to wind tunnel dimensions. Keeping TSR similitude ensures to have the same aerodynamic kinematics, as it is discussed in the following.

3.2. Model airfoil

One of the most critical aspect in the model blade design is the airfoil selection, as a matter of fact, the main limitation in reproducing the reference aerodynamic performance is related to the Reynolds number reduction when working at wind tunnel scales.

Referring to Eq. (3), Renyolds number depends on the air density ρ, wind speed U, the blade chord length c and air dynamic viscosity μ. The scale factor for Reynolds number is therefore defined as $\lambda_{Re} = \lambda_L \lambda_V$ equal to 150 (i.e. the wind tunnel Reynolds number is 150 times smaller the full scale one). This could result in a completely different aerodynamic behaviour of the blade profile at model scale.

$$Re = \frac{\rho \cdot V \cdot c}{\mu} \tag{3}$$

The Reynolds discrepancy forces to use different airfoil shape than the

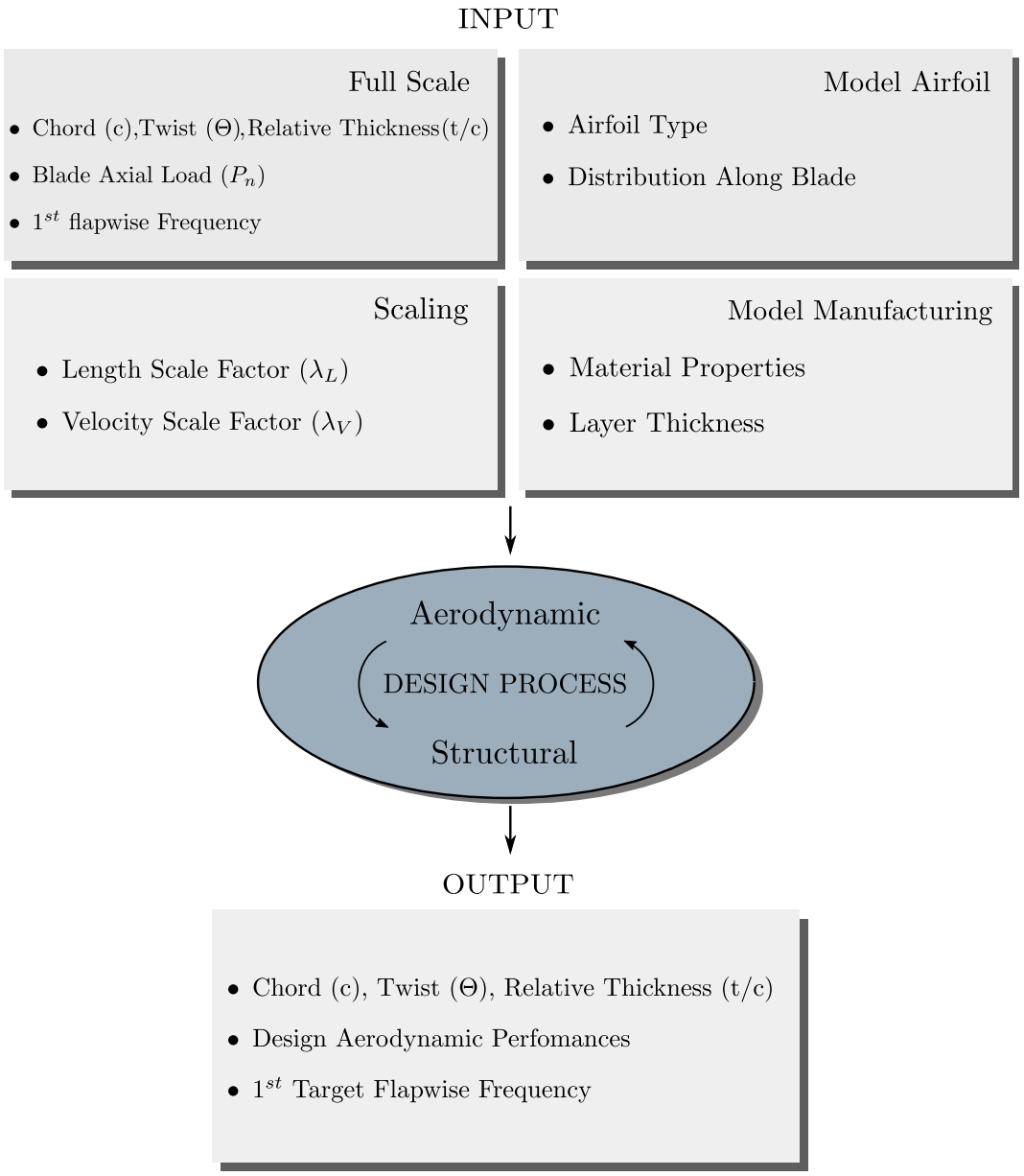

Fig. 1. Blade design I/O.

Table 3
Wind turbine operational parameters, V (m/s), Ω (RPM) and TSR (−).

V(10 MW)	Ω(10 MW)	TSR(10 MW)	V(model)	Ω(model)	TSR(model)
4.0	6.0	14.0	2.0	225.0	14.0
8.0	6.4	7.5	4.0	240.9	7.5
11.0	8.8	7.5	5.5	331.4	7.5
16.0	9.6	5.6	8.0	360.0	5.6
20.0	9.6	4.5	10.0	360.0	4.5
24.0	9.6	3.7	12.0	360.0	3.7

one used by DTU at full scale. In particular, choice went on the SD70xx airfoil series from the Selig-Donovan low Reynolds database (Lyon et al., 1998). From similar previous experience (Bredmose et al., 2015), the selected airfoil was the SD7032: Fig. 2 reports the model airfoil shape and the DTU 10 MW one at tip. The SD7032 has a thickness over chord length of roughly 10%, whereas the FFA-W3-240 thickness is 24%. The lower thickness leads to limited structural performance but it also makes the airfoil less sensible to flow separation at low Reynolds value conditions, like the ones encountered in the wind tunnel testing.

The aerodynamc coefficients for the SD7032 for Reyndolds numbers equal to 100×10^3 and 300×10^3 are available in (Lyon et al., 1998). However, for more suitable Reynolds number data, a new series of wind tunnel tests were performed on a 2D section model of the airfoil. The 2D sectional model is 497 mm span-wise long and 130 mm chord-wise long; it was manufactured with the same carbon fiber technology used for the turbine blade final model, this ensured the correct reproduction of surface finish effect on the airfoil performance, as well as in terms of trailing edge effective thickness. Fig. 3 shows the two main parts made of carbon fiber (4 layers of 0.2 mm thickness), the wing ends and the external attachment rods were machined from steel. The central aluminium part includes a total of 32 pressure taps drilled directly on the surface.

Tests were carried out at the red wind tunnel facility located at the Lyngby DTU campus (Denmark), Fig. 4. Two aerodynamic coefficients were measured:

- blade section lift coefficient, Cl: data from pressure taps

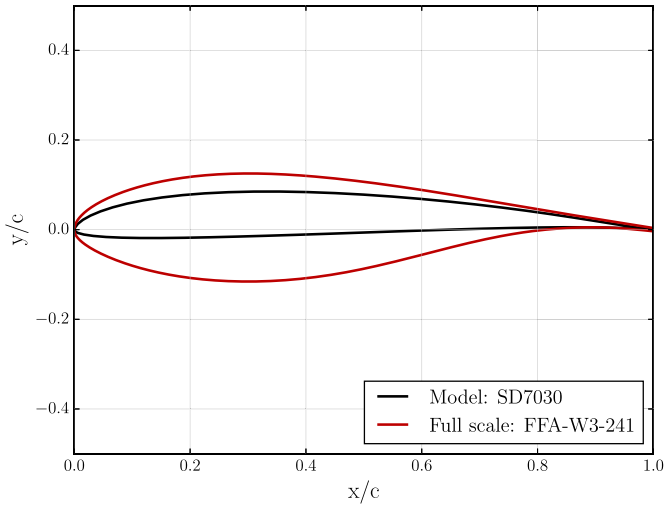

Fig. 2. Model airfoil (SD7032, solid line) and reference airfoil (FFA-W3-240, dashed line) shapes.

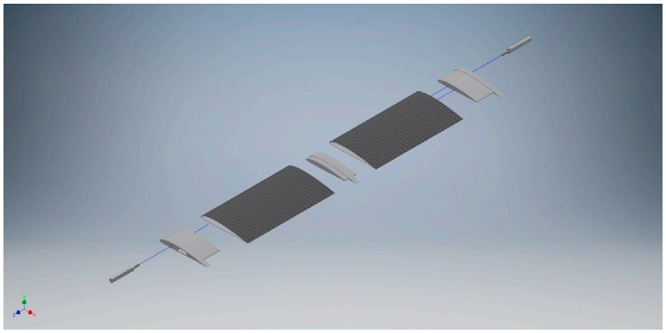

Fig. 3. 2D section model exploded-view drawing.

- blade section drag coefficient, Cd: data from wake rake pressure (placed downstream the model at around 5 chord length).

A total of eight Reynolds number were tested, $Re = [50 \times 10^3; 60 \times 10^3; 75 \times 10^3; 100 \times 10^3; 125 \times 10^3; 150 \times 10^3; 200 \times 10^3; 250 \times 10^3$. Figs. 5 and 6 show the obtained aerodynamic coefficients for SD7032 used in the aerodynamic design of the model blade for different Reynolds numbers; more details about the sectional tests can be found in (Lifes50+).

4. Design process

Standard turbine rotor design procedures are based on the blade element approach (Hansen, 2008; Manwell et al., 2009), starting from the hypothesis of no radial dependency of the results the design is carried out for each blade section independently. The developed procedure for the wind tunnel model design herein reported starts from the same blade element approach but instead of merely maximising the rotor aerodynamic performance, i.e. power efficiency, the design objective is the matching of a few selected parameters of the reference full scale turbine.

The aerodynamic and the structural optimization were carried out in combination, in an iterative loop, until the design reaches an optimal solution.

4.1. Aerodynamic design

The aerodynamic design deals with the definition of the chord and twist value distribution of the model blade. In order to match the DTU 10 MW scaled thrust value, it is necessary to match the scaled lift value along the blade, since in common working condition, the section normal load, P_n, is generated almost entirely by the section lift, as in Fig. 12.

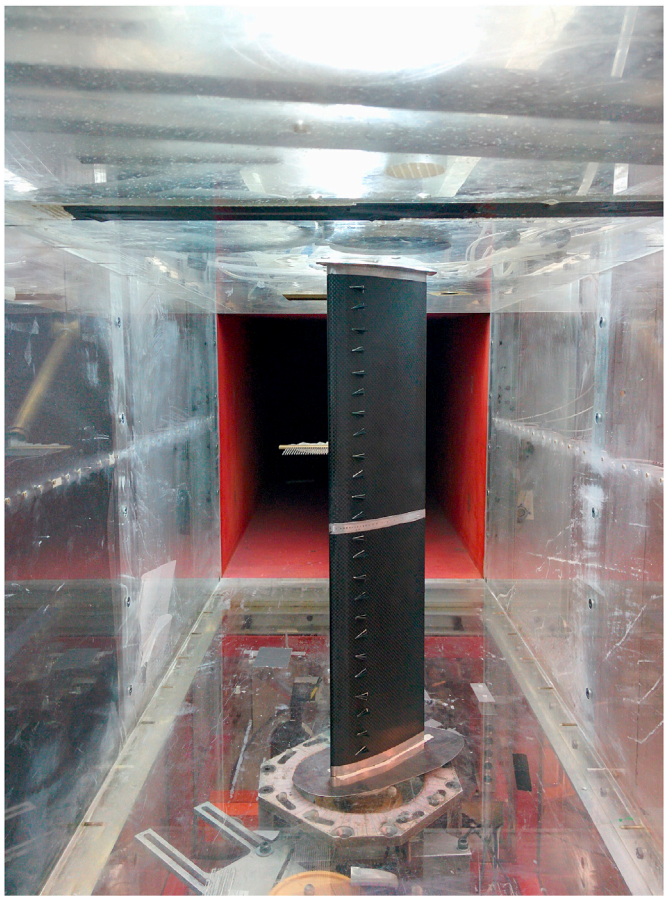

Fig. 4. DTU red wind tunnel test section.

The wind tunnel model is successfully designed if the model section lift L_{wtm} equals the scaled reference one, L_{10MW}, along the entire blade span, Eq (4).

$$\frac{L_{10MW}}{\Lambda_V^2 \Lambda_L} = L_{wtm} \tag{4}$$

So that it is necessary to consider section lift matching and same working condition for the reference and the model turbine (i.e. same TSR).

The flow angle at full scale and model scale must be exactly the same. It is well accepted (Hansen, 2008) to consider the induction factor of the wake, a and a' in Fig. 12, only influenced by the lift force and TSR. Therefore, it is possible to define an unique flow angle ϕ for both the reference and the model turbine, Eq. (5). For the model design it was considered the same pitch angle, θ, of the reference turbine and two different twist angles, β_{10MW} and β_{wtm}, the angle of attack, α is defined consequently in Eq. (5).

$$\begin{aligned} \alpha_{10MW} &= \phi - (\theta + \beta_{10MW}) \\ \alpha_{wtm} &= \phi - (\theta + \beta_{wtm}) \end{aligned} \tag{5}$$

Eq. (6) comes from the substitution of the lift value in Eq. (4) with the lift coefficient, Cl, times the air dynamic pressure, $0.5\,\rho V_{10MW}^2$ at full scale and $0.5\,\rho V_{wtm}^2$ in wind tunnel:

$$0.5\rho\left(\frac{V_{10MW}}{\lambda_V}\right)^2 Cl_{10MW}(\alpha_{10MW})\frac{c_{10MW}}{\lambda_L} = 0.5\,\rho Vwtm^2 Cl_{wtm}(\alpha_{wtm})c_{wtm} \tag{6}$$

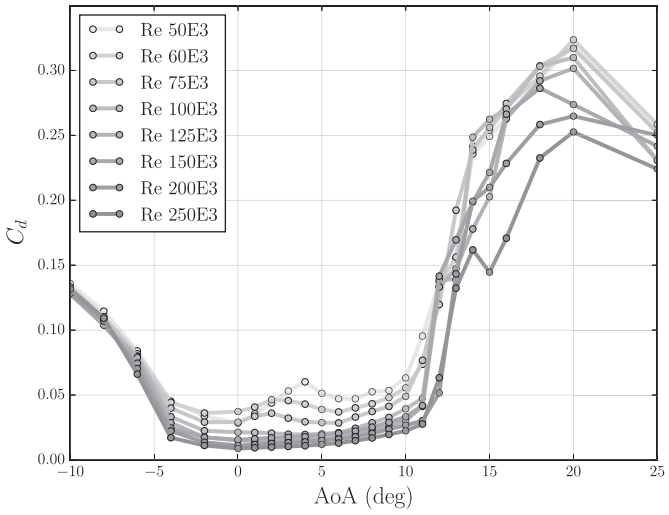

Fig. 5. SD7032 drag coefficients from DTU red wind tunnel test.

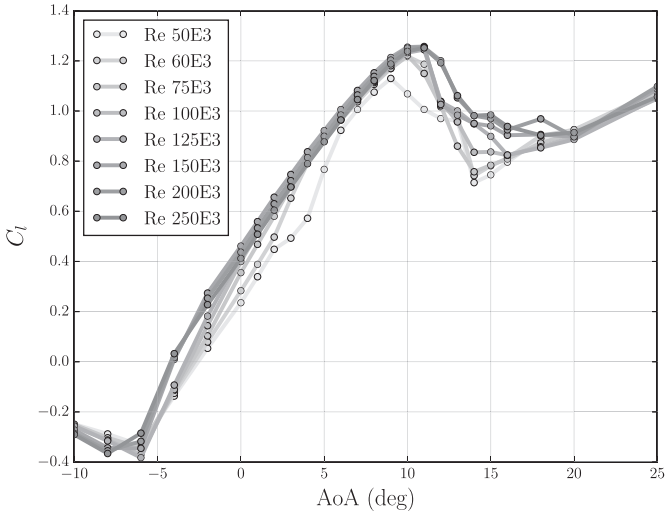

Fig. 6. SD7032 lift coefficients from DTU red wind tunnel test.

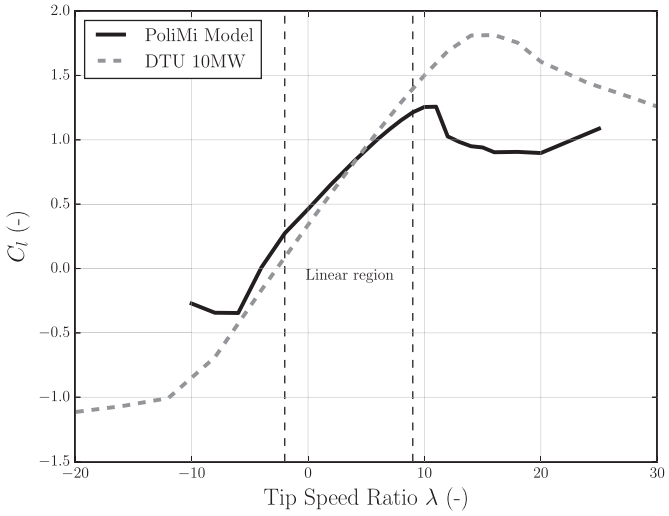

Fig. 7. Reference and model airfoil polar lift coefficient comparison, at rated condition for velocity scale factor $\lambda_V = 2$.

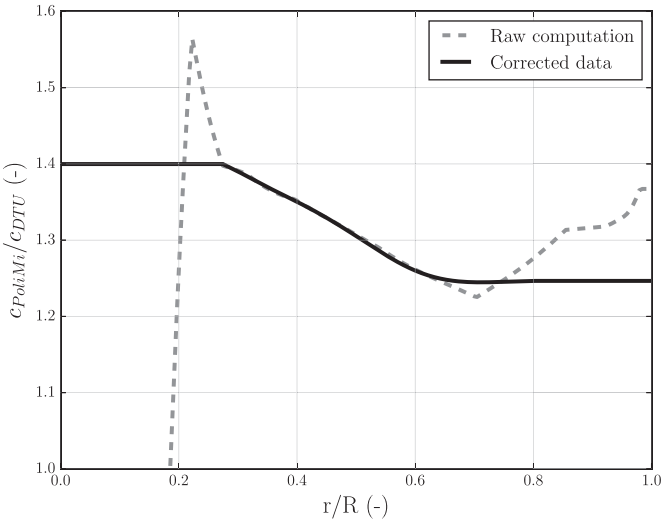

Fig. 8. RAW and corrected output of Eq. (11) as function of the non-dimensional blade station: model and scaled 10 MW chord ratio.

The Eq. (6) is simplified in Eq. (7).

$$Cl_{10MW}(\phi - (\theta + \beta_{10MW}))\frac{c_{10MW}}{\lambda_L} = Cl_{wtm}(\phi - (\theta + \beta_{wtm}))c_{wtm} \tag{7}$$

For pitch regulated turbines in standard working condition it is reasonable to consider that the blade is working away from stall at least in the region far from the hub. Therefore the blade is in the linear aerodynamic region and the lift coefficient can be well approximated with a linear curve with a Kl slope and Cl^0 zero value, Eq. (8).

$$\begin{aligned} Cl_{10MW}(\alpha_{10MW}) &= Kl_{10MW}\cdot\alpha_{10MW} + Cl^0_{10MW} \\ Cl_{wtm}(\alpha_{wtm}) &= Kl_{wtm}\cdot\alpha_{wtm} + Cl^0_{wtm} \end{aligned} \tag{8}$$

where Kl is the lift coefficient first derivative with respect to the angle of attack α in the airfoil linear region and Cl^0 is the lift coefficient value at null angle of attack.

Substituting this in Eq. (6) the first aerodynamic constraint equation is found, Eq. (9).

$$\begin{aligned} &\left(Kl_{10MW}\cdot(\phi - (\theta + \beta_{10MW})) + Cl^0_{10MW}\right)\cdot\frac{c_{10MW}}{\lambda_L} \\ &= \left(Kl_{wtm}\cdot(\phi - (\theta + \beta_{wtm})) + Cl^0_{wtm}\right)\cdot c_{wtm} \end{aligned} \tag{9}$$

Also the lift derivative with respect to the flow angle, ϕ, is imposed to be matched by the model design, in Eq. (10).

$$Kl_{10MW}\cdot\frac{c_{10MW}}{\lambda_L} = Kl_{wtm}\cdot c_{wtm} \tag{10}$$

This is done in order to ensure that the unsteady behaviour of the turbine is well reproduced by the model since the turbine is also going to be tested for unsteady condition (Bayati et al., 2016a). Moreover, it is reasonable to consider that, by first approximation, the unsteady behaviour of an aerodynamic body function of the first derivatives of the drag and lift curves calculated around the steady angle of attack (Cheli and Diana, 2015).

The Eqs. (9) and (10) can be rearranged in the final governing system Eq. (11) from which the model chord and twist are computed along the entire blade span.

$$\begin{cases} c_{wtm} = \dfrac{c_{10MW}}{\lambda_L}\cdot\dfrac{Kl_{10MW}}{Kl_{wtm}} \\ \beta_{wtm} = \beta_{10MW} - \dfrac{Cl^0_{10MW}}{Kl_{10MW}} + \dfrac{Cl^0_{wtm}}{Kl_{wtm}} \end{cases} \tag{11}$$

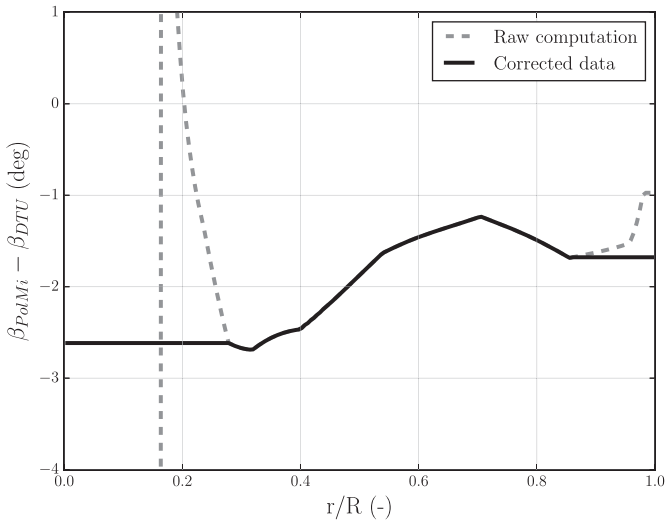

Fig. 9. RAW and corrected output of Eq. (11) as function of the non-dimensional blade station: model and 10 MW twist difference.

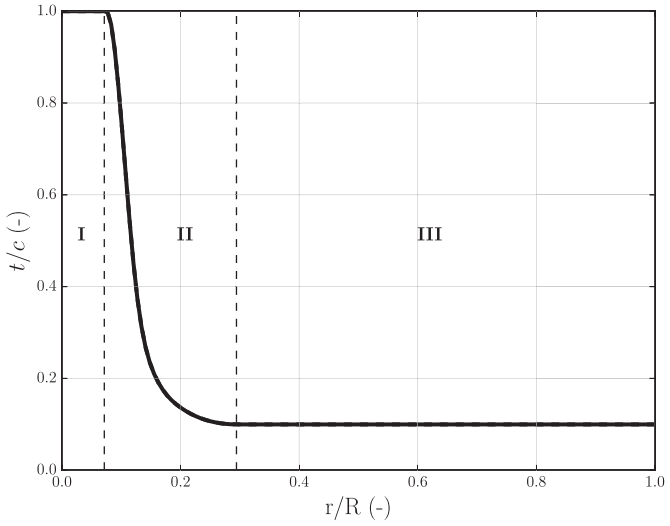

Fig. 10. Model blade t/c definition.

Table 4
Reference structural permanences.

Mode	reference frequency (Hz)	scaled frequency (Hz)
1st flap mode	**0.61**	**22.87**
1st edge mode	0.93	34.87
2nd flap mode	1.74	65.25
2nd edge mode	2.76	103.50

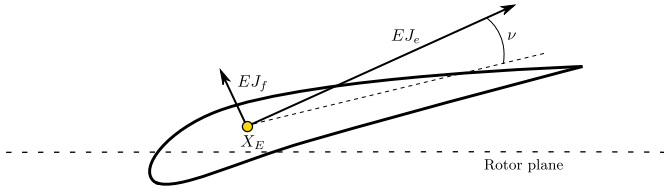

Fig. 11. Definition of the blade structural principal axes (not in scale).

In Fig. 7 the model airfoil, SD7032, is compared with the DTU 10 MW tip airfoil, FFA-W3-240 in terms of lift coefficient Cl versus angle of attack, for the range $-2 + 9$. The lift slope for the DTU airfoil is higher than the model one, thus the ratio Kl_{10MW}/Kl_{wtm} is greater than one which implies a model chord bigger than the geometric scaled reference one.

Fig. 8 reports the ratio between the model chord and the scaled reference value, Fig. 9 reports the difference between model twist and the reference one. The dashed line are the raw calculation output, the calculation results near the root region were discarded since calculation output seemed inconsistent by visual inspection. Also the tip region design has been simplified to a constant chord and pitch variation also due to manufacturing issues. The chord output was also interpolated with a cubic smoothing spline.

4.2. Structural design

The aerodynamic design defined the chord and twist distribution along the blade span. The remaining degree of freedom is the blade cross section relative thickness distribution (t/c). There are two constraints in the blade relative thickness definition:

- t/c at the blade tip is equal to the nominal t/c of the SD7032 airfoil (t/c = 10%)
- t/c must converge to 100% at the blade root to match the circular root section

The blade t/c is defined in three different regions reported in Fig. 10. Region I is the root region where the blade has a circular cross-section, region III is the tip region, where the cross-section is the SD7032 profile and lastly in the transition region II the cross-section must converge from the circular shape to the SD7032 shape.

The extension of region I was defined by technological constraints, in particular, a machined aluminium component has to be glued to blade root in order to allow a proper blade assembly. The remaining parameter is the transition region extension, l^{II}. This dimension has a great impact in the structural performance of the blade, it is obvious that higher l^{II} means higher model blade stiffness since the second moment of area of the circular section is greater than the SD7032 one.

The l^{II} length has been numerically optimized in order to ensure the matching of the first scaled flapwise blade frequency (Table 4). A *Matlab*® implemented beam FEM model code was iteratively ran until the correct first flapwise blade modal frequency. The FEM model is discretized by 193 beam elements, for each one the correspondent properties of blade section is assigned, the model is constrained as a cantilever beam in order to compute the modal analysis.

As reported in Fig. 11, from a structural point of view, the blade section is characterized by:

- $EJ_1(N{\cdot}m^2)$ bending stiffness about the first principal axis, flapwise direction
- $EJ_2(N{\cdot}m^2)$ bending stiffness about the second principal axis, edgewise direction
- $X_E(m)$ elastic section center.
- $\nu(rad)$ principal axes orientation with respect to the chord line
- $m(kg/m)$ mass per unit length

At this design phase the blade was considered made only by unidirectional high modulus carbon fiber layer aligned with the blade radial direction. Discarding the anisotropy in the material the elastic modulus and the density of the carbon fiber was taken from standard commercially available data ($E = 135\ MPa$, $\rho = 1560\ kg/m^3$). One layer of carbon fiber was considered for a total thickness of 0.26 mm. Knowing the material properties and thickness and considering the blade chord and twist output from the aerodynamic design the blade section mechanical properties were easily computed, see (Hansen, 2008) for theoretical details. The center of mass for each section is assumed to be coincident with the geometric center (isotropy).

Once the l^{II} length is optimized, the t/c blade profile is completely

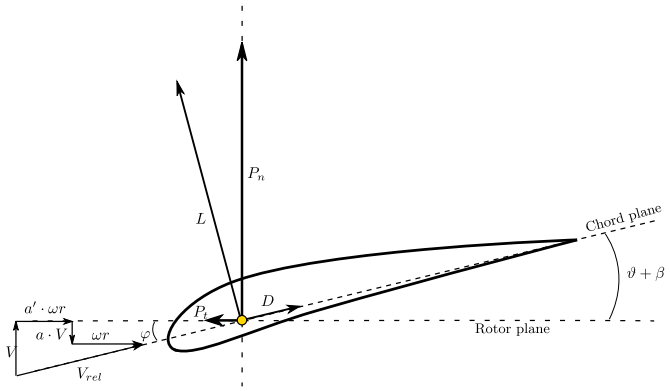

Fig. 12. Blade section velocities and loads.

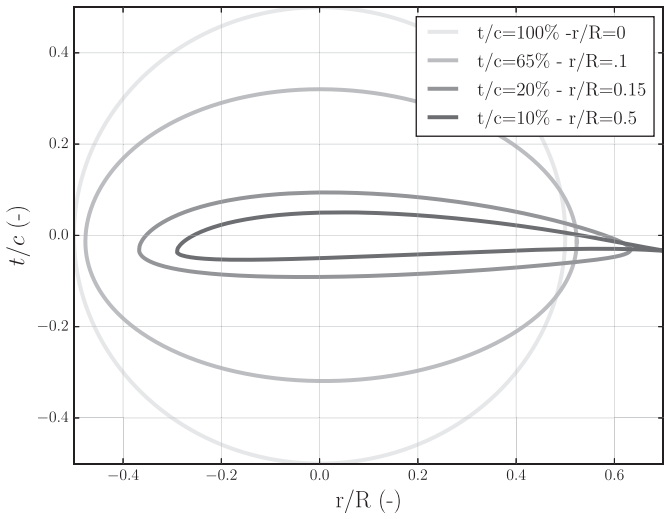

Fig. 13. Section shape at different radial position and t/c: section shape.

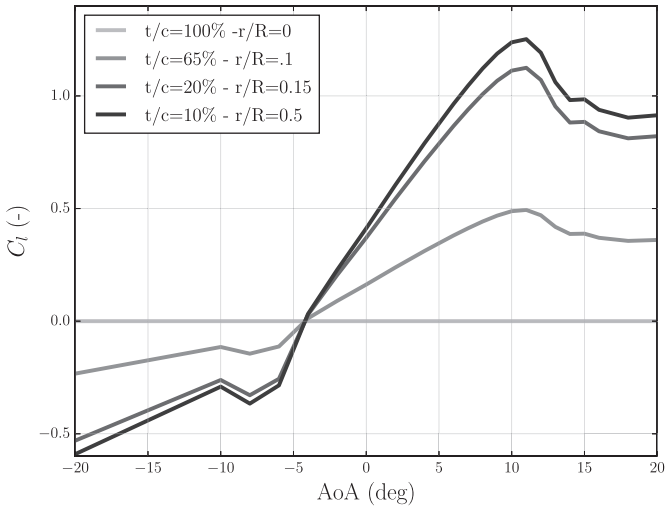

Fig. 14. Section lift coefficient at different radial position and t/c: section lift coefficient.

defined and the last phase of the structural design is the recalculation of the blade section shape and aerodynamic coefficient. In region I and region III the section shape and aerodynamic are perfectly known, being respectively equal to the circular section and SD7032 section. In region II, the section shape and aerodynamic coefficients are calculated as function of the radial position from simple linear interpolation based on the t/c local value. In Figs. 13 and 14 the section shape and lift coefficient are shown for four different radial blade positions.

4.3. Design loop

The aerodynamic and structural design are part of an iterative loop whose steps are summarized as follows:

1. Computing model airfoil Kl_{wtm} and Cl^0_{wtm} from model section lift coefficient
2. Calculating model chord and twist from Eq. (11)
3. Estimating section mechanical properties
4. Optimizing l^{II} for blade flapwise frequency
5. Updating blade section shape and lift coefficient and loop from (1)

The design is considered done when the l^{II} variation from one iteration to the following is below 5%. Fig. 15 shows the output of four subsequent iterations, the design starts from the DTU 10 MW reference value for chord, twist and t/c, then the optimized solution is computed. It is visible how the chord grows higher than the fullscale reference, in particular near the maximum chord position, the twist is almost equally reduced along the blade by a couple of degrees and the t/c curve goes more rapidly to the tip airfoil thickness than the 10 MW one.

4.4. Design numerical validation

The aerodynamic response of the designed scaled blade was checked using the AeroDyn module of NREL FAST software (Moriarty and Hansen, 2005). AeroDyn is one of the most used, freely available, rotor aerodynamic solver both in industry and academic research projects. For this application the main settings that has been adopted, are reported:

- no stall model;
- Equil inflow model (standard BEM theory (Hansen, 2008));
- Prandtl hub and tip loss factors;
- $\rho = 1.225(kg/m^3)$; $\nu = 1.45e^{-}5(m^2/s)$.

A total of 23 equally spaced wind speeds, ranging from cut in to cut out, were simulated for both DTU 10 MW and wind tunnel model. Fig. 16 shows, as an example, the output of the simulations in terms of thrust coefficient (the axes are scaled dimensions). The agreement is fairly good in particular up to the rated wind speed (condition of maximum thrust) thus the scaled blade design was considered a success, even more considering the strong Reynolds discrepancy and the completely different airfoils (e.g. efficiency) used in the scaled model design.

4.5. Blade shape export to CAD file

From the chord, twist and t/c distributions the blade shape is entirely known, at first step the blade is generated as a points cloud generated by 721 point at 193 different blade radial position (Fig. 17). The blade shape was converted to *iges* file format, from a point cloud, using a 3D B-Spline space interpolation based on a in-house *Matlab*® blades converter, for a direct manufacturing implementation.

4.6. Blade production

From the blade CAD file a CNC machined mould was realized, Fig. 18. The blades, Fig. 19, were realized with prepreg using a vacuum bag oven process, the mould is divided into two parts that are the pressure and suction side of the blade, the blade layers are placed in the mould and pushed against the mould surface with an inflated plastic balloon. The final carbon fiber layup differs from the design one for purely technological reasons: a 90 deg glass fiber layer is added to the single unidirectional carbon fiber one, in order to add some torsional stiffness to

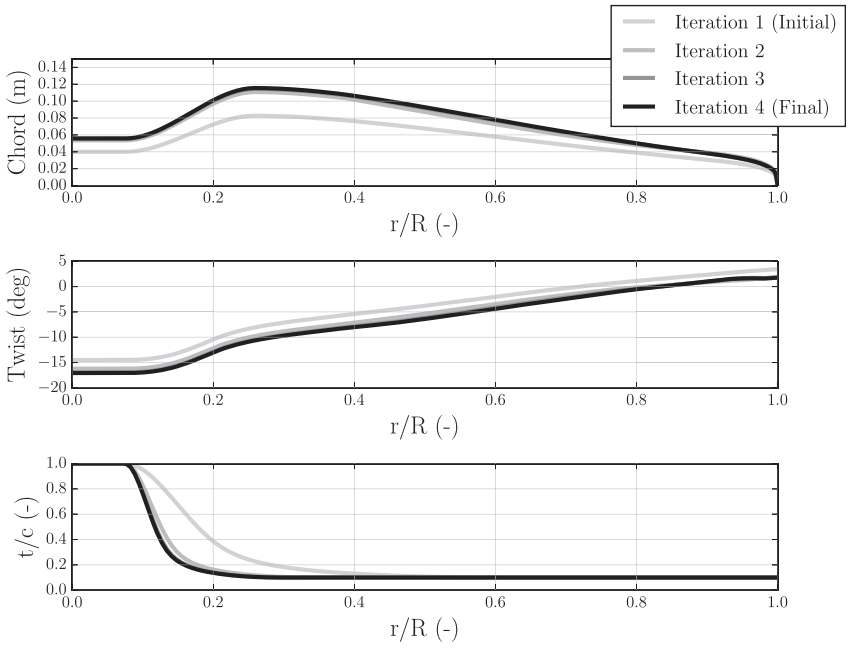

Fig. 15. Output of the design algorithm at different iteration loop as chord, twist and t/c value vs the non dimensional blade radial position.

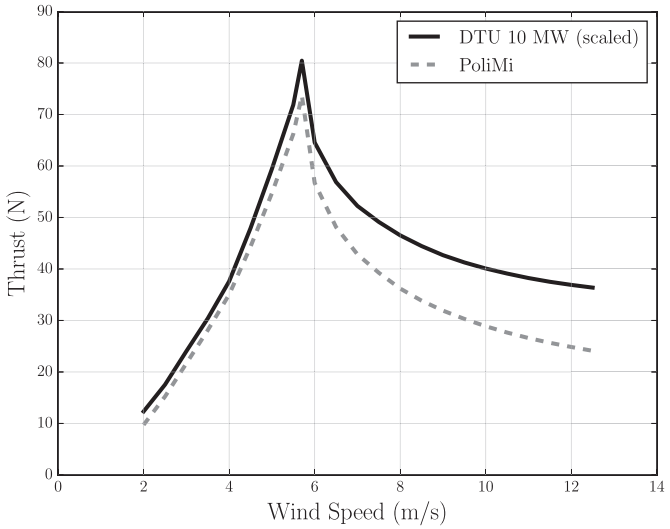

Fig. 16. Comparison of the thrust coefficient computed using FAST, for a velocity scale factor $\lambda_V = 2$, nominal (scaled) rotational speed and nominal pitch angle.

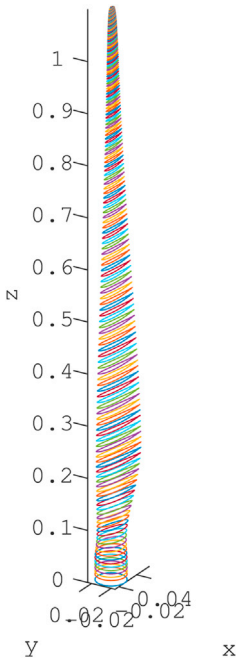

Fig. 17. Blade points cloud.

produced blade. The manufactured blade has a weight of 230 g, thus more then double of the target mass. It could have been possible to reduce further the weight of the blade using thinner carbon fiber layer but the main limitation was related to possible issues in the extraction phase of the model from the mould.

5. Design verification

5.1. Modal analysis

The model blade has been structurally examined using a modal analysis approach. The authors performed an impulse response test using a series of piezoelectric accelerometer and an instrumented hammer. The blade was constrained to the ground through a rigid beam in a cantilever configuration, as visible in Fig. 20.

A limited number of accelerometers were employed not to have an excessive mass compared to the blade, and placed at different distance from the blade constrained section. Table 5 reports the precise indication of the accelerometers displacement in the span-wise direction, the disposition is nearly equally spaced, while the sensors distances from the leading edge were varied from one sensor to the other. This "zig-zag" disposition was employed in order to have a sensing pattern able to discern torsional from bending modes.

A series of impact tests responses were acquired, the impact position was at 0.1 m from the blade root, exciting the blade in a point close to the grounded section ensure that the first flap-wise modes will be excited by the impact. From the impact tests the mode shapes of the first two blade

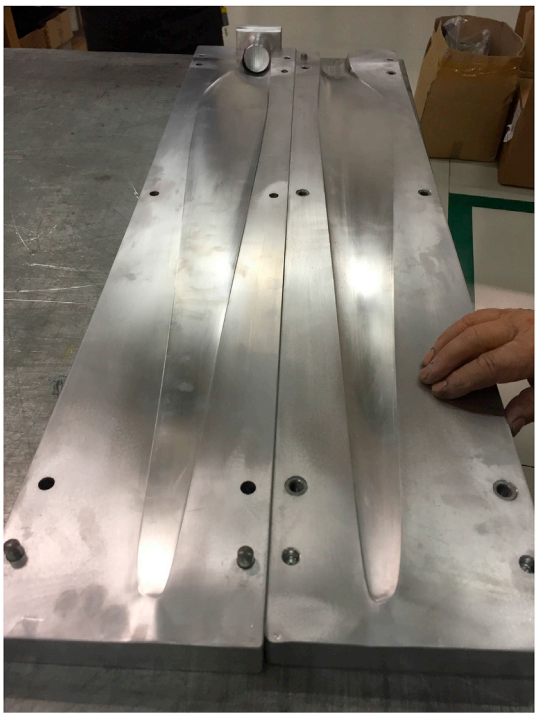

Fig. 18. Aluminium mould.

Fig. 19. Carbon fiber blades.

modes were reconstructed, looking at Figs. 21 and 22 the displacement is compatible with pure flapwise modes, the two mode are respectively the first and second flapwise mode.

The experimental estimated modes frequencies are slightly lower than the scaled design ones, this could be a consequence of the different layer layup and more importantly of the overweight of the produced blade. Table 6 reports the relative error between the design and measured frequencies for the first two flapwise modes.

In order to deal with the lower natural frequency of the manufactured blade than expected (Table 6), the chance of modifying the scaling factor of the model was taken into consideration. As explained in Sec.2, for this particular application the velocity scale, λ_V, could be varied in a limited range and looking at Table 2 the frequency scale, λ_f, is inversely proportional to the velocity scale so an higher λ_V will turn out in lower scaled model frequency.

Table 7 reports the design versus measured frequency considering a $\lambda_V = 3$ and thus a $\lambda_f = \lambda_L \lambda_V^{-1} = 25$. For this velocity scales the blade is more rigid then expected but the error on the first flpawise mode, which is the most important issue for the aero-elastic response of the turbine, is now close to 10% that is considered by the authors a good result, also confirmed by the performance of the rotor in wind tunnel tests at greater velocity scale factor with respect the design one, as explained in the following. More details can also be found in (Bayati et al., 2017a).

5.2. Wind tunnel tests

The wind tunnel tests were performed in the Polimi wind tunnel using a model of the entire turbine described in details in (Bayati et al., 2016b), focusing, as first step, on the steady aerodynamic characterization.

Firstly, test with $\lambda_V = 2$ was performed, Figs. 23 and 24 show the results of the wind tunnel model compared to the scaled DTU 10 MW performance in terms of thrust and torque. The agreement on the thrust force is excellent for all the tested conditions, the maximum thrust force, $\sim 70N$, is well reproduced by the turbine model. Also the torque matching, that was not the main model target, is very good up to maximum tested wind speed at the rated condition.

Figs. 25 and 26 report the same results at $\lambda_V = 3$, so at lower wind tunnel speed. In this case an higher discrepancy was observed between the measured performance and the reference ones, possibly due to the Reynolds number decrease. In order to correct the discrepancy in the results, different collective pitch angle values were tested, between -1 deg and -5 deg from the nominal pitch angle. It was possible to get the experimental curve closer to the reference one, in fact the model thrust curve almost matches the target values but this was done at expense of the torque matching (lowering the pitch angle the thrust increases while the torque decreases). However, this could be accepted since the thrust matching is the primary design goal.

Beside the steady aerodynamic curves, wind tunnel tests allowed for a first analysis of the unsteady scaled model response (Bayati et al., 2016a). As stated in Sec.4.1, the aerodynamic design of the scaled blade was done comparing the lift coefficient derivatives of the full scale and the model scale airfoil, this should ensure that the unsteady response of the scaled turbine due to dynamic variation of the operational parameters is similar to the DTU 10 MW one. In order to check the unsteady response, a linearization approach was used both numerically and experimentally: a small wind speed variation was imposed at different mean wind speed without changing the rotor speed or the blade pitch. The variation in the thrust force was computed numerically, using the FAST model of the DTU 10 MW and of the scaled model one, as well as sampled during the wind tunnel tests. Fig. 27 shows the computed or acquired variation of thrust force at four mean wind speed condition:

1. Below Rated ($V = 2.33$ m/s at wind tunnel scale);
2. Rated ($V = 3.67$ m/s at wind tunnel scale);
3. Above Rated ($V = 5.33$ m/s at wind tunnel scale);
4. Above Rated 2 ($V = 6.67$ m/s at wind tunnel scale

Looking at the results it is possible to notice how the derivatives of the thrust force are very similar between numerical model of the full scale and model scale turbine as well as for the measured wind tunnel response of the model turbine. This confirms the effective design approach for wind turbine rotors to be tested in wind tunnel with the aim of

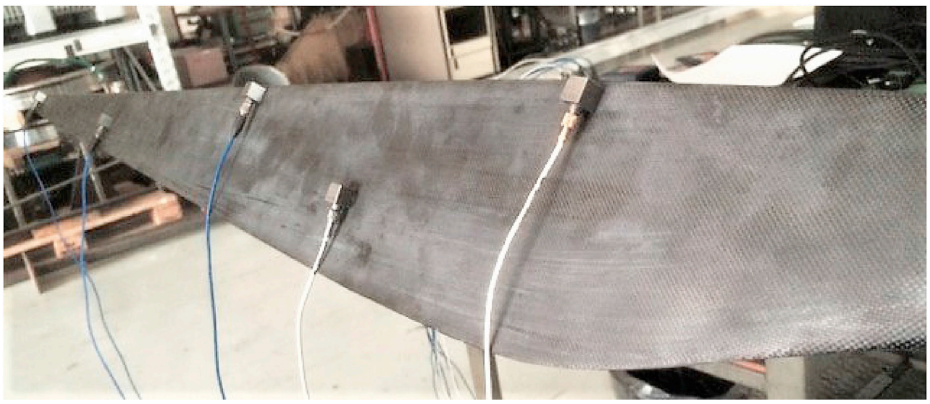

Fig. 20. Experimental setup.

Table 5
Accelerometers position details.

accelerometer number	position	span-wise distance from root (m)	distance from leading edge (m)
Acc1	PosA	0.23	0
Acc2	PosB	0.38	0.066
Acc3	PosA	0.52	0
Acc4	PosA	0.77	0.036
Acc5	PosA	1.08	0

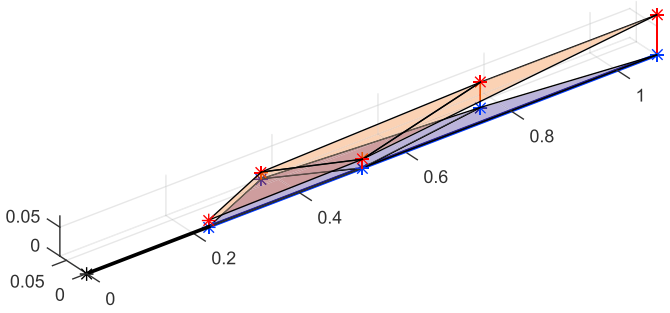

Fig. 21. First mode shape.

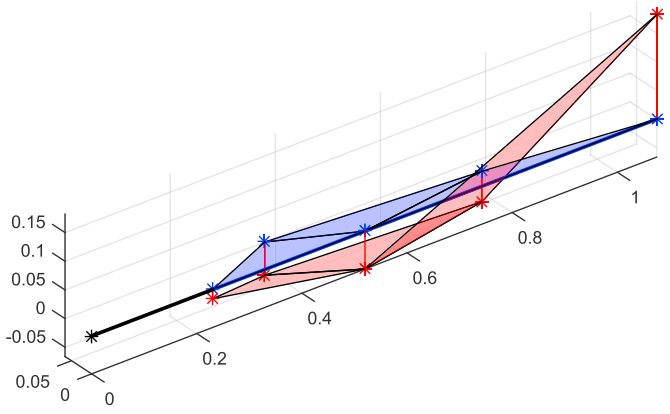

Fig. 22. Second mode shape.

investigating also the aerodynamics of floating offshore wind turbines, where the unsteady phenomenon become relevant, see (Bayati et al., 2017b; Bachynski et al., 2015).

Table 6
Comparison between design and measured blade frequencies.

Mode	Design frequency (Hz)	Experimental frequency (Hz)	Relative error
1st flap mode	22.87	17.1	−25.5%
2nd flap mode	65.25	56.4	−13.6%

Table 7
Comparison between design and measured blade frequencies (using $\lambda_V = 3$, $\lambda_f = 25$).

Mode	Design frequency (Hz)	Experimental frequency (Hz)	Relative error
1st flap mode	15.25	17.1	12.1%
2nd flap mode	65.25	56.4	29.6%

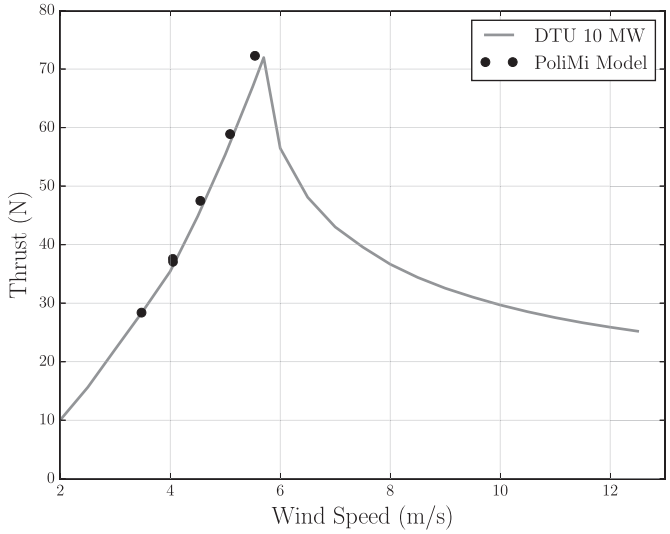

Fig. 23. Wind tunnel test results compared with the reference scaled DTU 10 MW performance: thrust.

6. Conclusions

The paper reported the design methodology for an aero-elastic scale rotor of a 10 MW wind turbine. Theoretical and technical aspects were discussed and the satisfactory experimental verification of such a design was commented, revealing an effective approach for this kind of application. The wind tunnel tests have shown the very good aerodynamics performance, in particular considering that the main target of the design was the matching of the DTU 10 MW thrust curve. The

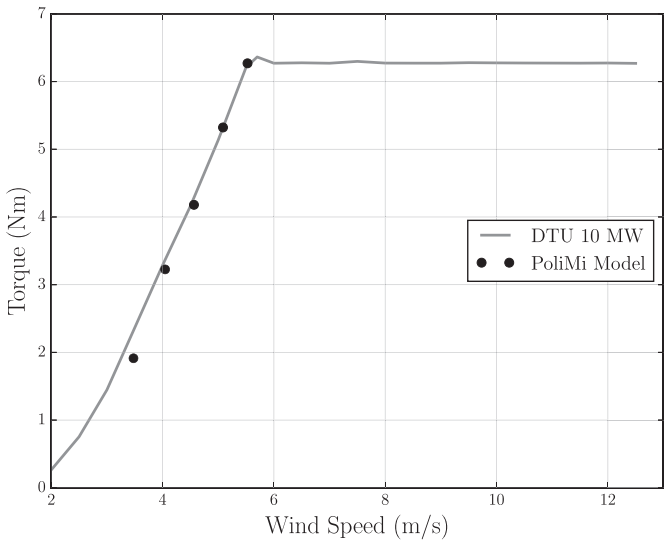

Fig. 24. Wind tunnel test results compared with the reference scaled DTU 10 MW performance: torque.

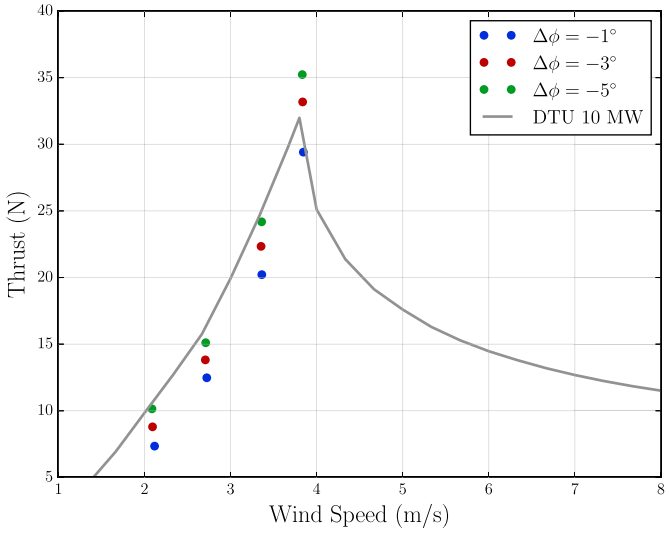

Fig. 25. Wind tunnel test results, for $\lambda_V = 3$: thrust.

velocity scale factor $\lambda_V = 2$ was taken as reference for the aero-elastic design, and the related wind tunnel results have shown excellent agreement with the target. Furthermore, also an other velocity scale factor, $\lambda_V = 3$, was assessed during the test, showing very good agreement as well, although inevitably a bit worse than the initial target. However, tuning the collective pitch of the blades, the objective of matching the target thrust is reached, also for $\lambda_V = 3$. Furthermore, assuming $\lambda_V = 3$ test configuration, also the first flapwise natural frequency of the blade, assessed experimentally through the reported modal analysis, is consistent beside the non-quantifiable variables in the actual manufacturing process that can be hardly accounted in the design phase. Therefore, in these conditions, the scaled rotor can be considered consistent in an aero-elastic sense. Furthermore, it has been shown that good agreement between the target and the experimental aerodynamic derivatives of the thrust force, makes the model reliable in the dynamic response about a given dynamic state (i.e. linearization) with important outcome in the investigation of floating offshore wind turbine dynamics.

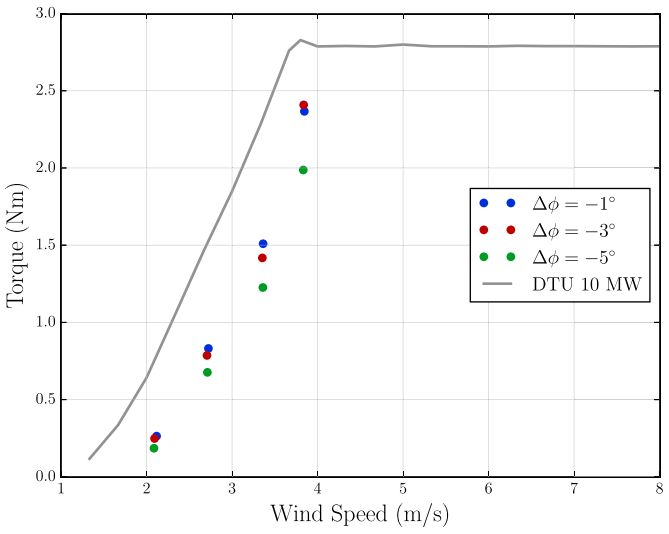

Fig. 26. Wind tunnel test results, for $\lambda_V = 3$: torque.

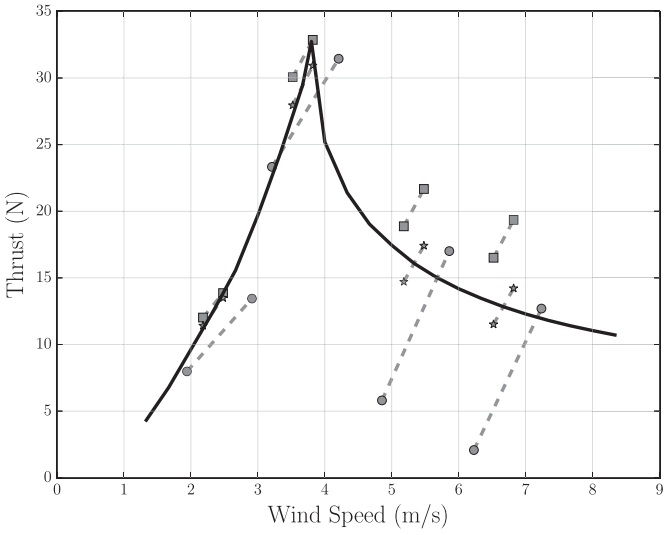

Fig. 27. Thrust variation due to wind speed variation. ∘ - wind tunnel; ∗ - DTU 10 MW FAST model; □ - scaled rotor FAST model; dashed line - reference DTU 10 MW steady thrust.

Acknowledgements

This project has received funding from the European Union's Horizon 2020 research and innovation programme under grant agreement No 640741.

References

Bachynski, E., Chabaud, V., Sauder, T., 2015. Real-time hybrid model testing of floating wind turbines: sensitivity to limited actuation. Energy Procedia 80, 2–12. http://dx.doi.org/10.1016/j.egypro.2015.11.400.

Bak, C., Bitsche, R., Yde, A., Kim, T., Hansen, M.H., Zahle, F., …, Behrens, T., 2012. Light Rotor: the 10-MW reference wind turbine. In: Proceedings of EWEA 2012-European Wind Energy Conference. European Wind Energy Association (EWEA).

Bak, C., et al., 2013. The DTU 10-MW Reference Wind Turbine. Technical University of Denmark, DTU Wind Energy, Denmark.

Bayati, I., Belloli, M., Facchinetti, A., Giappino, S., 2013. Wind tunnel tests on floating offshore wind turbines: a proposal for hardware-in-the-loop approach to validate numerical codes. Wind Eng. 37 (6), 557–568. http://dx.doi.org/10.1260/0309-524X.37.6.557.

Bayati, I., Belloli, M., Ferrari, D., Fossati, F., Giberti, H., 2014. Design of a 6-DoF robotic platform for wind tunnel tests of floating wind turbines. Energy Procedia. http://dx.doi.org/10.1016/j.egypro.2014.07.240.

Bayati, I., Belloli, M., Bernini, L., Zasso, A., October 2016a. "Wind tunnel validation of AeroDyn, within LIFES50+ project: imposed Surge and Pitch tests. J. Phys. Conf. Ser. 753 (5) http://dx.doi.org/10.1088/1742-6596/753/9/092001.

Bayati, I., Belloli, M., Bernini, L., Fiore, E., Giberti, H., Zasso, A., October 2016b. On the functional design of the DTU10 MW wind turbine scale model of LIFES50+ project. J. Phys. Conf. Ser. 753 (5) http://dx.doi.org/10.1088/1742-6596/753/5/052018.

Bayati, I., Belloli, M., Bernini, L., Giberti, H., Zasso, A., 2017. On the scale model technology for floating offshore wind turbines. IET Renew. Power Gener. http://dx.doi.org/10.1049/iet-rpg.2016.0956. IET Digital Library.

Bayati, I., Belloli, M., Bernini, L., Zasso, A., 2017. A formulation for the unsteady aerodynamics of floating wind turbines, with focus on the global system dynamics. In: 36th International Conference on Ocean, Offshore and Arctic Engineering, Trondheim (Norway). OMAE2017–61925.

Bottasso, C.L., Campagnolo, F., Petrović, V., 2014. Wind tunnel testing of scaled wind turbine models: beyond aerodynamics. J. Wind Eng. Ind. Aerodyn. 127, 11–28. http://dx.doi.org/10.1016/j.jweia.2014.01.009. ISSN 0167-6105.

Bredmose, H., Mikkelsen, R., Hansen, A.M., Laugesen, R., Heilskov, N., Jensen, B., Kirkegaard, J., 2015. Experimental study of the DTU 10 MW wind turbine on a TLP floater in waves and wind. In: EWEA Offshore 2015 Conference, Copenhagen.

Bredmose, H., 2014. Contribution to InnWind Deliverable 4.22, Scaling Laws for Floating Wind Turbine Testing. DTU Wind Energy.

Campagnolo, F., Bottasso, C., Bettini, P., 2014. Design, manufacturing and characterization of aero-elastically scaled wind turbine blades for testing active and passive load alleviation techniques within a ABL wind tunnel. In: The Science of Making Torque from Wind.

Cheli, F., Diana, G., 2015. Advanced Dynamics of Mechanical Systems. Springer.

H2020 Lifes50+ Project official website: http://lifes50plus.eu.

Hansen, M.O.L., 2008. Aerodynamics of Wind Turbines, second ed. Earthscan Publications Ltd.

Jonkman, J., Butterfield, S., Musial, W., Scott, G., 2009. Definition of a 5-MW Reference Wind Turbine for Offshore System Development. Technical Report NREL/TP-500–38060. NREL National Renewable Energy Laboratory.

Lyon, C.A., Broeren, A.P., Gigure, P., Gopalarathnam, A., Selig, M.S., 1998. Summary of Low-speed Airfoil Data, vol. 3. SoarTech Publications, Virginia Beach, VA.

Make, M., 2014. Predicting Scale Effects on Floating Offshore Wind Turbines. MsC thesis. TUDelft.

Manwell, J., McGowan, J., Rogers, A., 2009. Wind Energy Explained: Theory, Design and Application, second ed. John Wiley & Sons, Ltd.

Moriarty, P.J., Hansen, C., 2005. AeroDyn Theory Manual, vol. 15. National Renewable Energy Laboratory NREL, p. 50036313 no. January.

Zasso, A., Giappino, S., Muggiasca, S., Rosa, L., 2005. Optimization of the boundary layer characteristics simulated at Politecnico di Milano Boundary Layer Wind Tunnel in a wide scale ratio ranges. IRIS Politecnico di Milano.